This article has been accepted for publication in a future issue of this journal, but has not been fully edited. Content may change prior to final publication. Citation information: DOI 10.1109/TIE.2018.2864695, IEEE Transactions on Industrial Electronics

Stability Analysis of PV Generators with Consideration of P&O Based Power Control

Yanghong Xia, *Student Member, IEEE*, Wei Wei, Miao Yu, *Member, IEEE* and Peng Wang, *Fellow, IEEE*

***Abstract*—The photovoltaic (PV) generators are continuously increasing in recent years, whose power is usually controlled through the perturbation and observation (P&O) method. In essence, the P&O method is nonlinear and discontinuous. Hence, the conventional small-signal stability analysis is unsuitable anymore when the influence of the P&O based power control is considered. Focusing on this problem, this paper adopts the nonlinear describing function (DF) method to conduct the accurate stability analysis of PV generators with consideration of P&O based power control. The detailed procedures about the DF method are introduced, then the related influence factors like perturbation size, filters and so on are analyzed quantitatively. Furthermore, the comparison with the conventional stability analysis methods is made, which suggests that the DF method can effectively enhance the accuracy of the stability analysis. All the conclusions are verified by the real-time hardware-in-loop (HIL) tests.**

***Index Terms*—PV generators, describing function, P&O method, stability analysis.**

I. INTRODUCTION

PHOTOVOLITATIC (PV) generators are considered as promising renewable energy sources to replace the conventional and exhaustible fossil energy sources because of their cleanliness and abundance almost anywhere [1], [2]. Therefore, the installed capacity of PV generators is continuously increasing both in the centralized way (large PV power stations) and the distributed way (ac microgrids or dc microgrids) in recent years [3]-[5]. To better facilitate the integration of PV generators, the proper power control is necessary, among which the perturbation and observation (P&O) method is widely used due to its simplicity and adaptability. It only requires measurements of i_{pv} and v_{pv}, and it is capable of tracking the reference power or the maximum power quite accurately according to the upper dispatch [6].

The stability of PV generators is the foundation to ensure the successful integration and to realize the desired performance of power regulation. However, the P&O method is nonlinear and discontinuous, to which the conventional small-signal stability analysis cannot be applied anymore. The existing methods almost take no consideration of the influence of the P&O based power control.

Viewing the PV side as an ideal dc voltage source, some simplified stability analyses are conducted to study the interaction between the PV generators and the power network [7]-[13]. In [7], the *d*-*q* small-signal impedances of the grid-tied inverter used to integrate PV generators and other renewable energy sources into three-phase power system are analyzed. It is found that the *q*-*q* channel impedance presents a negative resistance feature, which will influence the stability of the grid-tied inverter. To solve this kind of instability issue, a novel impedance controller is proposed in [8] to reshape the *q*-axis impedance into a positive resistance in the low-frequency band. Then, the stable margin of the gird-tied inverter is enhanced. In [9], based on the assumption that the PV side is the constant voltage source, through the state space model and the eigenvalue analysis, it is found that the angle droop control can improve the stability of PV generators when regulating the active power. Because of the dc nature, the PV generators can have higher efficiency when they are integrated into the dc microgrid. In consequence, the stability of dc microgrid has gotten some attention, where the PV generators are viewed as current or power sources to provide power for the microgrid [10]-[13]. Since the models of PV generators are simplified to a greater degree, lots of dynamics of the PV generators are omitted. Therefore, references [10]-[13] conclude that PV generators have no influence on the stability of dc microgrid, while the constant power loads will cause the instability issues due to their negative resistances. But according to the studies of this paper, if the detailed models of PV generators are taken into consideration, the PV generators will also induce some instability issues like the power oscillation and so on.

To improve the accuracy of the stability analysis, the dynamics of PV side are taken into consideration based on the small-signal models, but the discontinuous P&O based power control is still not considered [14]-[20]. In [14], the dynamics of the dc-link capacitor across the output terminal of the PV panel are taken into consideration, through the eigenvalue analysis and time-domain simulation, it is shown that the dc-link capacitor and its control strategy can introduce oscillatory modes in subsynchronous range of frequencies. For PV generators connected to the power system through the current-source converters, the corresponding small-signal model is established in [15]. The related results reflect that the current-source converter based PV generators have stable performance

This work is supported in part by the National Key R&D Program of China (2017YFB0902002), in part by the Zhejiang Provincial Key R&D Program (2017C01039).

The authors Y. Xia, W. Wei and M. Yu are with the College of Electrical Engineering, Zhejiang University, Hangzhou, 310027, China (e-mail: royxiayh@126.com; wwei@zju.edu.cn; zjuyumiao@zju.edu.cn).

The author P. Wang is with the School of Electrical and Electronic Engineering, Nanyang Technological University, Singapore (e-mail: epwang@ntu.edu.sg).

This article has been accepted for publication in a future issue of this journal, but has not been fully edited. Content may change prior to final publication. Citation information: DOI 10.1109/TIE.2018.2864695, IEEE Transactions on Industrial Electronics

under different operating conditions and following sudden variations in insolation level with proper power synchronization control. In [16] and [17], the stability of the hybrid wave and PV power generation system is analyzed. In this process, the models of renewable energy sources are considered, but the power control in the outer loop is omitted. Hence, the results are not very accurate especially when these heterogeneous energy sources need to be coordinated by different power control strategies. Taking the randomness of irradiance into consideration, a probabilistic small-signal analysis approach is proposed in [18] and [19] to study the dynamic stability of grid-tied PV generators. This method pays more attention to the randomness of irradiance, but does not consider the detailed power control for the PV generators, where the power control is simplified as a constant voltage control strategy. Hence, the results will be not very accurate too. In [20], to avoid the discussion about the discontinuous P&O based power control, an impedance shaping method based on sliding-mode control is designed. The nonlinear discontinuous hysteretic comparator is simplified through only considering the ideal system dynamics in the sliding-mode surface. Then, the reduced model is used for the stability analysis.

Through the above narration, the existing methods about the stability analysis of PV generators can be classified into two categories,

1) **C1**: The PV side is just viewed as an ideal dc voltages source. Then, the stability analysis of PV generators is focused on the control algorithms of grid-side converters. This process completely omits the dynamics of PV panels and the corresponding power control. The system model can be reduced at utmost and it is suitable for the stability analysis of the large-scale PV generators system. At the same time, the corresponding results are not very accurate and lots of factors of instability issues will be neglected.

2) **C2**: The PV side is modeled, but the influence of the nonlinear discontinuous P&O based power control is not considered. This process is usually based on small-signal model, hence, the nonlinear discontinuous P&O based power control cannot be modeled directly according to the Taylor's expansion. Compared to the first category, the accuracy of results is enhanced, but it still loses many dynamics. Therefore, it cannot provide design guidance for some critical parameters like perturbation size and it cannot explain some unstable phenomena reasonably.

In order to provide accurate and complete results about the stability analysis including power control, converter control and so on, a nonlinear describing function (DF) method is adopted in this paper to analyze the stability of a PV generator connected to a dc power system in detail. Through the DF method, the frequency-domain model of the nonlinear discontinuous P&O based power control can be established, through which the influence of the power control can be studied quantitatively. Based on the complete frequency-domain model of the studied PV generator system, the related influence factors like perturbation size, filters and so on are analyzed. Then, it is found that the P&O based power control contributes a lot in the dynamics of the system. And some unstable issues like the power oscillation can be explained successfully by the proposed analysis method, while the conventional stability analysis methods cannot illustrate the reasons effectively. That is, the proposed DF method considering the influence of the power control can effectively enhance the accuracy of the stability analysis. All the conclusions are verified by the real-time HIL tests based on the RTLAB and the TMS320F28335 DSP.

The remainder of this paper is organized as follows. In Section Ⅱ, the fundamental principle of the DF method is introduced. In Section Ⅲ, the complete model of the studied PV generator is established in the frequency domain. After that, the detailed stability analysis is conducted in Section Ⅳ. Then, the related results of the HIL tests are presented and discussed in Section Ⅴ. At last, the conclusions are drawn in Section Ⅵ.

II. Principle of the Describing Function Method

In this paper, the DF method is adopted to analyze the stability of the PV generators with consideration of P&O based power control. DF method is an effective way to study the stability of nonlinear system especially with some discontinuous elements [21], [22]. Compared to the small-signal analysis method which is a kind of time-domain approximation methods, the DF method is a kind of frequency-domain approximation methods.

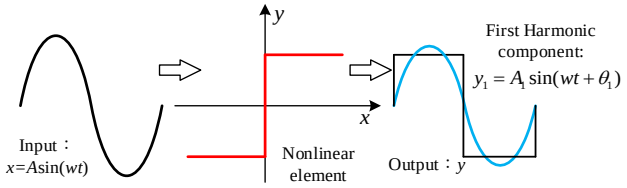

Fig.1. Response of the nonlinear element.

The fundamental principle of the DF method is to obtain the first harmonic component of the output when the nonlinear element is excited with sinusoidal signal input. As shown in Fig.1 where the nonlinear element is a sign function, assuming that the input is $x = A\sin(wt)$, the output is y, which is also a periodic signal. The output y can be expanded according to Fourier series as

$$y = A_0 + \sum_{k=1}^{\infty} A_k \sin(kwt + \theta_k). \quad (1)$$

There are two assumptions as follows to further conduct the DF method,

1) If the nonlinear element is odd-symmetric, the dc component A_0 is zero.

2) If the linear part of the system is low-pass, the higher harmonics can be neglected.

Hence, only the first harmonic component needs to be considered. Then, the approximate transfer function of the nonlinear element $N(A)$ can be obtained by the ratio of the first harmonic component and the input sinusoidal signal. That is,

$$N(A) = \frac{A_1 e^{j\theta_1}}{A}. \quad (2)$$

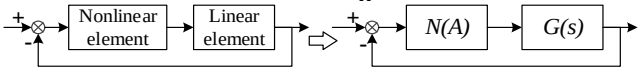

Fig.2. Equivalent control block diagram based on the DF method.

The whole system can be approximatively transformed into a linear system in the frequency domain with a variable gain

This article has been accepted for publication in a future issue of this journal, but has not been fully edited. Content may change prior to final publication. Citation information: DOI 10.1109/TIE.2018.2864695, IEEE Transactions on Industrial Electronics

amplifier $N(A)$ as shown in Fig.2, where $G(s)$ is the transfer function of the linear part. The modified Nyquist criterion can be used to judge stability of the system, which is similar to the Nyquist criterion of the linear system just substituting (-1, j0) with $-1/N(A)$. If $G(s)$ is the minimum phase system, the modified Nyquist criterion can be expressed as follows,

1) If $-1/N(A)$ is not surrounded by $G(s)$, the system is stable like Fig.3 (a).

2) If $-1/N(A)$ is surrounded by $G(s)$, the system is unstable like Fig.3 (b).

3) If $-1/N(A)$ intersects with $G(s)$, the system is critical stable. For the intersection point with amplitude A_a, if the system is unstable in the region $[A_a - \Delta A,\ A_a)$ and is stable in the region $(A_a, A_a + \Delta A]$ where $\Delta A \ll A_a$, the intersection point is the stable oscillation point like the point a in Fig.3 (c). Or else, the intersection point is the unstable oscillation point like the point b in Fig.3 (c).

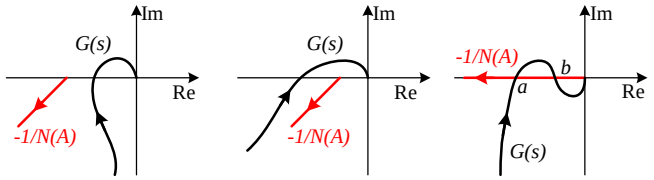

Fig.3. Relative position of $-1/N(A)$ and $G(s)$. (a) Stable. (b) Unstable. (c) Critical stable.

III. Modeling of the PV Generator

This section mainly establishes the model of the studied PV generator connected to the dc power system with consideration of the P&O based power control. As shown in Fig.4, the PV panel is connected to the dc power system such as dc microgrid through a buck dc/dc converter. The capacitance across the PV terminal is C_{pv}, the output current and terminal voltage of the PV panel are $v_{pv}$and i_{pv} respectively. The dc/dc converter is filtered through a LC filter, whose inductance is L and capacitance is C respectively. The corresponding inductive current is i_L and capacitive voltage is v_o. The output current injecting to the network is i_o. The dc power system is modeled as a voltage source with impedance L_s and R_s (including line impedance).

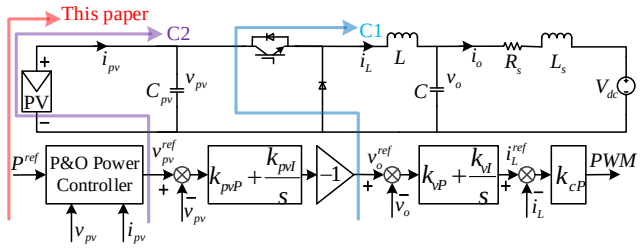

Fig.4. Topology and control strategy of the studied PV generator. And the research scope of the existing stability analysis methods, **C1**: Viewing the PV side as an ideal voltage source; **C2**: Without consideration of the P&O based power control.

The whole control strategy consists of three parts. The outermost loop is the P&O based power controller, which can overcome the intermittency and nonlinearity of the PV generator and also generates the reference value v_{pv}^{ref} for the PV voltage controller. The new grid code regulations require that the PV generators must inject the constant power into the grid to provide reserve service and avoid adverse effects of PV generators with high penetration like overloading the grid [23]-[24]. That is, if P^{ref} is greater than the maximum power of the PV generator, the PV generator outputs the maximum power. If the P^{ref} is less than the maximum power of the PV generator, the PV generator should output the power P^{ref}. Hence, the studied P&O based power control is with function of constant power generation. The detailed flow chart is shown in Fig.5, where the perturbation size is ε and power control cycle is T_p.

Then, the PV voltage controller makes the terminal voltage of the PV panel v_{pv} track the reference value v_{pv}^{ref} accurately. The innermost loop is the output voltage controller, which makes the output voltage v_o track the reference value v_o^{ref} accurately.

As mentioned in the Introduction Section, the existing stability analysis methods can be summarized as two categories namely,

C1: Viewing the PV side as an ideal voltage source;

C2: Considering the dynamics of the PV side but without consideration of the P&O based power control.

Their research scopes are clearly illustrated in the Fig.4. Also, the research scope of this paper is illustrated.

According to Fig.4, the model of the PV generator can be derived as

$$\begin{cases} \frac{1}{2}C_{pv}\frac{dv_{pv}^2}{dt} = P_{pv} - dv_{pv}i_L \\ L\frac{di_L}{dt} = dv_{pv} - v_o \\ C\frac{dv_o}{dt} = i_L - i_o \\ L_s\frac{di_o}{dt} = -R_s i_o + v_o - V_{dc} \end{cases}, \tag{3}$$

where P_{pv} is the output power of the PV panel and d is the duty ratio.

Assuming the equilibrium points of the system are $(V_{pv}^*, I_L^*, V_o^*, I_o^*, D^*)$, then the small-signal model can be obtained as

$$\begin{cases} C_{pv}\frac{d\Delta v_{pv}}{dt} = k\frac{\Delta v_{pv}}{V_{pv}^*} - \Delta d I_L^* - \Delta i_L D^* - \frac{\Delta v_{pv}}{V_{pv}^*}D^* I_L^* \\ L\frac{d\Delta i_L}{dt} = \Delta d V_{pv}^* + \Delta v_{pv}D^* - \Delta v_o \\ C\frac{d\Delta v_o}{dt} = \Delta i_L - \Delta i_o \\ L_s\frac{d\Delta i_o}{dt} = -R_s\Delta i_o + \Delta v_o \end{cases}, \tag{4}$$

where $\Delta P_{pv} = k\Delta v_{pv}$.

Through the model of the PV panel [25], [26], the coefficient k can be calculated as

$$k = N_P(I_{sc} + K_I\Delta T)(G/G_N) - \frac{N_P(I_{sc}+K_I\Delta T)}{\exp((V_{oc}+K_V\Delta T)/V_t a)-1}\left[\exp\left(V_{pv}^*/N_S V_t a_D\right)(V_{pv}^*/N_S V_t a_D + 1) - 1\right], \tag{5}$$

where N_P and N_S are the numbers of series- and parallel-modules. I_{sc} and V_{oc} are the open-circuit voltage and short-circuit current of a PV model. V_t is the thermal voltage and a_D is the ideality constant of the equivalent diode. G and $G_N$are the actual irradiance and the nominal irradiance respectively. $\Delta T = T - T_N$, T and T_N are the actual temperature and the nominal

This article has been accepted for publication in a future issue of this journal, but has not been fully edited. Content may change prior to final publication. Citation information: DOI 10.1109/TIE.2018.2864695, IEEE Transactions on Industrial Electronics

temperature respectively. K_I and K_V are the current and voltage coefficients respectively. From the power-voltage curve in Fig.6, it can be seen that on the left side, $k > 0$, on the right side, $k < 0$.

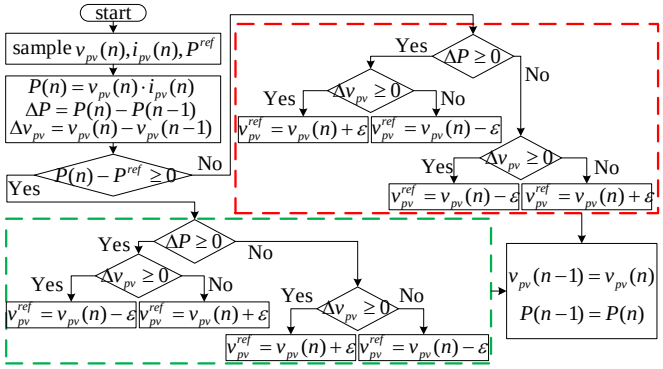

Fig.5. P&O based power control.

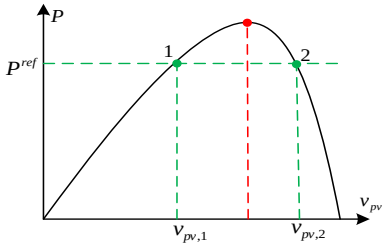

Fig.6. Power-voltage curve of the PV panel.

The corresponding equivalent points can be calculated as

$$\begin{cases} P_{pv}^* = V_{pv}^* N_P (I_{sc} + K_I \Delta T)[\frac{G}{G_N} - \frac{\exp(V_{pv}^*/N_S V_t a_D) - 1}{\exp((V_{oc} + K_V \Delta T)/V_t a_D) - 1}] \\ V_o^* = 0.5 * (V_{dc} + \sqrt{V_{dc}^2 + 4 P_{pv}^* R_s}) \\ D^* = V_o^*/V_{pv}^* \\ I_L^* = I_o^* = P_{pv}^*/V_{pv}^* D^* \end{cases}, \quad (6)$$

where P_{pv}^* or V_{pv}^* is chosen as a known variable about the steady operation point.

In the following, we will establish the model of the nonlinear discontinuous P&O based power controller. As shown in Fig.5, the output of the power controller can be expressed as

$$v_{pv}^{ref} = \frac{\varepsilon}{T_P} \int \mathrm{sgn}(P^{ref} - P_n)\mathrm{sgn}(\Delta P)\mathrm{sgn}(\Delta v) dt, \quad (7)$$

where $\mathrm{sgn}(x) = 1$ if $x \geq 0$, $\mathrm{sgn}(x) = -1$ if $x < 0$.

Ignoring the sampling errors and combining Fig.6, it can be concluded that

$$\begin{cases} \mathrm{sgn}(\Delta P)\mathrm{sgn}(\Delta v) = 1, & left\ side\ of\ Fig.6 \\ \mathrm{sgn}(\Delta P)\mathrm{sgn}(\Delta v) = -1, & right\ side\ of\ Fig.6 \end{cases}. \quad (8)$$

Hence, (7) can be simplified as

$$\begin{cases} v_{pv}^{ref} = \frac{\varepsilon}{T_P} \int \mathrm{sgn}(P^{ref} - P_n) dt, & left\ side \\ v_{pv}^{ref} = -\frac{\varepsilon}{T_P} \int \mathrm{sgn}(P^{ref} - P_n) dt, & right\ side \end{cases}. \quad (9)$$

Combining (4), the control strategy in Fig.4 and (9), the complete small-signal model of the PV generator connected to the dc power system can be derived, whose block diagram is shown in Fig.7.

Fig.7 shows the complete small-signal model of the PV generator with consideration of the nonlinear discontinuous P&O based power control when the operating point is located on the left side. The model when the operating point is located on the right side can be also obtained only needing to reverse the sign function. Through the model in Fig.7, it can be seen that the whole system can be divided into two parts namely the nonlinear part $N(A)$and the linear part $G(s)$. The structure of Fig.7 is the same as the structure of Fig.2. It is obvious that the model in Fig.7 meets the two assumptions when the DF method is applied. That is, the nonlinear part is odd-symmetric and the linear part of the system is low-pass. Hence, after obtaining the DF $N(A)$ of the nonlinear part and the transfer function $G(s)$of the linear part, the stability of the whole system can be analyzed in detail according to the modified Nyquist criterion introduced in the Section Ⅱ.

IV. Detailed Stability Analysis

This section mainly conducts the detailed stability analysis according to the criterion introduced in the Section Ⅱ and the model established in Section Ⅲ.

According to the definition, the DF of the sign function can be calculated as

$$N(A) = \frac{4}{\pi A}. \quad (10)$$

Now calculating *G(s)*, based on (4), the following equations can be obtained

$$\begin{cases} \Delta v_{pv} = H_{pv}(s)\Delta d \\ \Delta v_o = H_{vo}(s)\Delta d \\ \Delta i_L = H_{iL}(s)\Delta d \end{cases}, \quad (11)$$

where $H_{pv}(s)$, $H_{vo}(s)$ and $H_{iL}(s)$ are shown in (12) at the bottom of this page. In these equations, $g_{pv} = (I_L^* D^* - k)/V_{pv}^*$.

From Fig.4 and Fig.7, Δd can be expressed as

$$\Delta d = \{[(\Delta v_{pv} - \Delta v_{pv}^{ref})PI_{pv} - \Delta v_o]PI_{vo} - \Delta i_L\}P_{iL}, \quad (13)$$

where PI_{pv}, PI_{vo} and P_{iL} are the corresponding controllers shown in Fig.7.

Combining (11), (13) and Fig.7, the linear part *G(s)* can be calculated as

$$G(s) = k\frac{\varepsilon/T_p}{s} \cdot \frac{H_{pv}(s)PI_{pv}PI_{vo}P_{iL}}{H_{pv}(s)PI_{pv}PI_{vo}P_{iL} - H_{vo}(s)PI_{vo}P_{iL} - H_{iL}(s)P_{iL}}. \quad (14)$$

Then, if the system is critical stable which means that $-1/N(A)$ intersects with $G(s)$, the oscillation amplitude A_o and frequency w_o can be calculated as

$$G_{Im}(w_o) = 0, N(A_o) = -1/G_{Re}(w_o), \quad (15)$$

where $G(jw) = G_{Re}(w) + jG_{Im}(w)$.

The type of the chosen PV module is KC200GT, whose detailed parameters are presented in [25], [26]. The PV panel is

$$\begin{cases} H_{pv}(s) = -\frac{LL_sCI_L^*s^3 + (L_sCV_{pv}^*D^* + LCI_L^*R_s)s^2 + [I_L^*(L+L_s) + CR_sV_{pv}^*D^*]s + (V_{pv}^*D^* + I_L^*R_s)}{LL_sCC_{pv}s^4 + (LCC_{pv}R_s - LL_sCg_{pv})s^3 + [L_sCD^{*2} + C_{pv}(L+L_s) - LCR_sg_{pv}]s^2 + [CR_sD^{*2} - g_{pv}(L+L_s) + C_{pv}R_s]s + (D^{*2} - R_sg_{pv})} \\ H_{vo}(s) = -\frac{-L_sC_{pv}V_{pv}^*s^2 + (L_sV_{pv}^*g_{pv} + L_sI_L^*D^* - C_{pv}V_{pv}^*R_s)s + (V_{pv}^*g_{pv} + I_L^*D^*)R_s}{LL_sCC_{pv}s^4 + (LCC_{pv}R_s - LL_sCg_{pv})s^3 + [L_sCD^{*2} + C_{pv}(L+L_s) - LCR_sg_{pv}]s^2 + [CR_sD^{*2} - g_{pv}(L+L_s) + C_{pv}R_s]s + (D^{*2} - R_sg_{pv})} \\ H_{iL}(s) = -\frac{-L_sCC_{pv}V_{pv}^*s^3 + (L_sCV_{pv}^*g_{pv} + L_sCI_L^*D^* - CC_{pv}V_{pv}^*R_s)s^2 + [CR_s(V_{pv}^*g_{pv} + I_L^*D^*) - C_{pv}V_{pv}^*]s + (V_{pv}^*g_{pv} + I_L^*D^*)}{LL_sCC_{pv}s^4 + (LCC_{pv}R_s - LL_sCg_{pv})s^3 + [L_sCD^{*2} + C_{pv}(L+L_s) - LCR_sg_{pv}]s^2 + [CR_sD^{*2} - g_{pv}(L+L_s) + C_{pv}R_s]s + (D^{*2} - R_sg_{pv})} \end{cases}. \quad (12)$$

This article has been accepted for publication in a future issue of this journal, but has not been fully edited. Content may change prior to final publication. Citation information: DOI 10.1109/TIE.2018.2864695, IEEE Transactions on Industrial Electronics

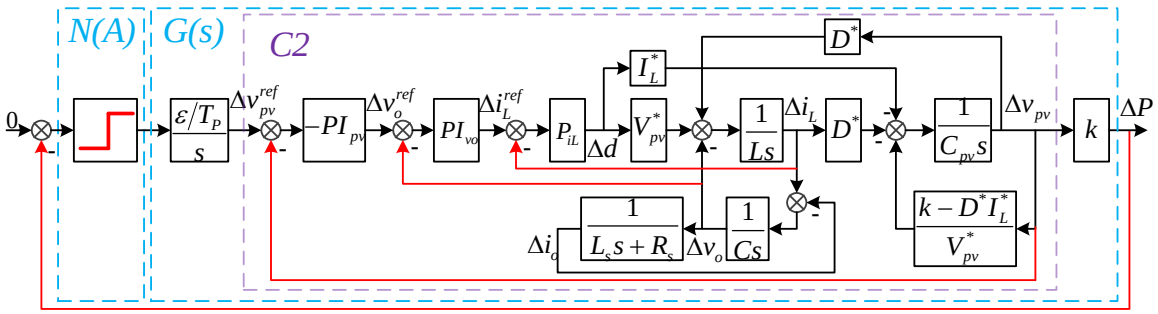

Fig.7. Complete small-signal model of PV generator with consideration of nonlinear discontinuous P&O based power control.

composed of 40 series and 30 parallel modules, whose maximum power can reach about 240 kW under the nominal operation conditions.

The other rated parameters are shown in Table Ⅰ. Then, the related information can be derived through these parameters.

Hereafter, several influence factors are studied including operation points, control parameters and so on. Also, the obtained results are compared with the conventional stability analysis method **C2** mentioned above namely considering the dynamics of the PV side but without consideration of the P&O based power control. The model of the **C2** method is from Δv_{pv}^{ref} to Δv_{pv} as illustrated through the purple dashed box in Fig.7, by which the close-loop transfer function $G_{C2}(s)$ can be directly obtained. It can be calculated as

$$G_{C2}(s) = sG(s)/(k\,\varepsilon/T_P). \tag{16}$$

Then, the stability based on the **C2** method can be simply analyzed through the distribution of zeros and poles of the obtained close-loop transfer function.

TABLE Ⅰ
RATED SYSTEM PARAMETERS

Parameters	Rated Value
C_{pv}, L, C, L_s, R_s	1.5 mF, 3 mH, 5 mF, 0.3 mH, 20 mΩ
V_{dc}	400 V
PI_{pv}	$k_{pvP} = 0.15$, $k_{pvI} = 40\ s^{-1}$
PI_{vo}	$k_{vP} = 3$ A/V, $k_{vI} = 200$ A/Vs
P_{iL}	$k_{cP} = 0.01$ V/A
T_P, ε	0.02 ms, 0.5 V
G, T	$G = 1000$ W/m^2 (G_N), $T = 298.16$ K (T_N)
P_{pv}^*, V_{pv}^*	180 kW, 731 V
k	245 W/V

A. *Operation Points*

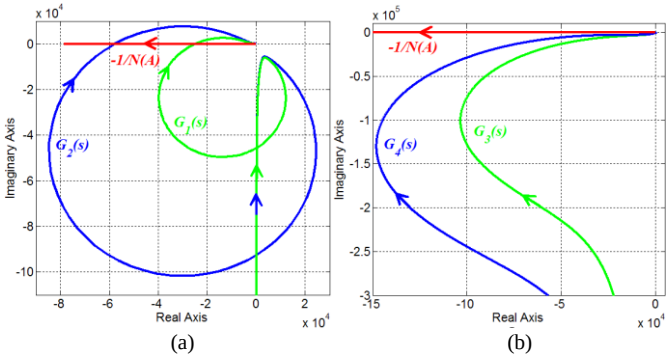

(a) (b)

Fig.8. Nyquist diagram of the system with changes of operation points. (a) Operation points (180 kW, 731 V) and (160 kW, 650 V) located on the left side. (b) Operation points (180 kW, 1253 V) and (160 kW, 1264 V) located on the right side.

This part mainly studies the influence of the operation points, which are indicated by (P_{pv}^*, V_{pv}^*). There are four operation points to be studied namely (180 kW, 731 V) and (160 kW, 650 V), (180 kW, 1253 V) and (160 kW, 1264 V). The first two points are located on the left side of the power-voltage curve, while the last two points are located on the right side.

For these operation points, the transfer functions $G(s)$of the linear part are as follows in sequence,

$$\begin{cases} G_1 = \dfrac{8.1*10^8(s+289.2)(s+266.7)(s+66.67)(s^2+86.96s+7.29*10^5)}{s(s+3195)(s+48.45)(s^2+13.24s+4.4*10^4)(s^2+568.1s+7.27*10^5)} \\ G_2 = \dfrac{7.2*10^8(s+323.7)(s+266.7)(s+66.67)(s^2+89.52s+7.28*10^5)}{s(s+2768)(s+49.08)(s^2+6.46s+4.9*10^4)(s^2+587.2s+7.36*10^5)} \\ G_3 = \dfrac{-5.4*10^9(s+298.2)(s+266.7)(s+66.67)(s^2+86.96s+7.29*10^5)}{s(s+5188)(s+706.5)(s^2+34.97s+1590)(s^2+585.2s+8.49*10^5)} \\ G_4 = \dfrac{-5.8*10^9(s+323.7)(s+266.7)(s+66.67)(s^2+89.52s+7.28*10^5)}{s(s+5094)(s+829)(s^2+30.06s+1352)(s^2+610.5s+8.63*10^5)} \end{cases} \tag{17}$$

Combining (10) and (17), the Nyquist diagram of the PV generator system can be depicted in Fig.8.

From Fig.8, it can be seen that when the operation point is located on the right side, the system is stable as Fig.8 (b) shows. But when the operation point moves to the left side, the system becomes critical stable as Fig.8 (a) shows. Furthermore, the intersection point is the stable oscillation point. The oscillation amplitude and frequency can be calculated according to (15) as follows

$$\begin{cases} A_1 = 32\ \text{kW}, w_1 = 221\ \text{rad/s} \\ A_2 = 86\ \text{kW}, w_2 = 227\ \text{rad/s} \end{cases}. \tag{18}$$

From (18), it can be concluded that with further moving to the left, the oscillation amplitude becomes much larger and the oscillation frequency changes a little.

On the other hand, according to (16) and (17), it can be seen that the close-loop poles of $G_{C2}(s)$ are all located in the left-half plane no matter the operation points are on the right or left side. Hence, through the **C2** method, the system is always stable, which contradicts the result of the proposed analysis method. But according to the actual experimental results in the next section, it can be found that the result of the proposed analysis method is more accurate.

B. *Control Parameters*

This part mainly studies the influence of the control parameters, where the proportional coefficient k_{pvP} of the PV voltage controller and the perturbation size ε of the P&O based power controller are chosen as the representative parameters. k_{pvP} can greatly influence the bandwidth and response speed of the inner loop, while ε can greatly influence the outer loop in the same way.

This article has been accepted for publication in a future issue of this journal, but has not been fully edited. Content may change prior to final publication. Citation information: DOI 10.1109/TIE.2018.2864695, IEEE Transactions on Industrial Electronics

When $k_{pvP} = 0.1, 0.15, 0.3$ in sequence, the corresponding transfer functions $G(s)$of the linear part are as follows,

$$\begin{cases} G_1 = \frac{5.4*10^8(s+400)(s+289.2)(s+66.67)(s^2+86.96s+7.29*10^5)}{s(s+2733)(s+49.1)(s^2-36.96s+4.7*10^4)(s^2+645.5s+7.77*10^5)} \\ G_2 = \frac{8.1*10^8(s+289.2)(s+266.7)(s+66.67)(s^2+86.96s+7.29*10^5)}{s(s+3195)(s+48.45)(s^2+13.24s+4.4*10^4)(s^2+568.1s+7.27*10^5)}, \\ G_3 = \frac{1.6*10^9(s+298.2)(s+133.3)(s+66.67)(s^2+86.96s+7.29*10^5)}{s(s+4577)(s+46.3)(s^2+116.3s+3.5*10^4)(s^2+412.3s+6.7*10^5)} \end{cases} \quad (19)$$

Combining (10) and (19), the Nyquist diagram can be depicted in Fig.9 (a).

When $\varepsilon = 0.1, 0.5, 1$ V in sequence, the corresponding $G(s)$ is similar to G_2 in (19) with different gain coefficients, whose Nyquist diagram is shown in Fig.9 (b).

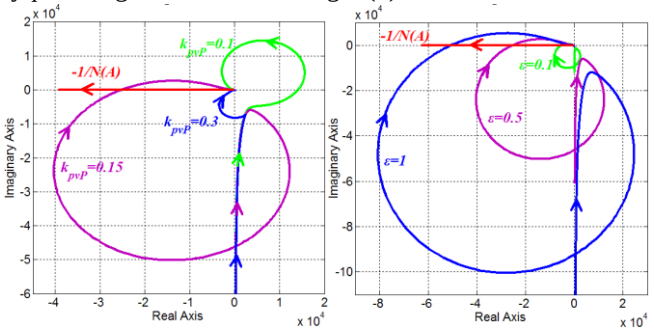

(a) (b)

Fig.9. Nyquist diagram of the system with changes of control parameters. (a) $k_{pvP} = 0.1, 0.15, 0.3$. (b) $\varepsilon = 0.1, 0.5, 1$ V.

When $k_{pvP} = 0.1$ that is the bandwidth of the inner loop is decreased, although $G_1(s)$ does not surround $-1/N(A)$ as shown in Fig.9 (a), $G_1(s)$ has two poles in the right-half plane. According to the Nyquist criterion, the system is unstable. This conclusion coincides with the result of **C2** method since $G_1(s)$ has unstable poles. With the increase of k_{pvP} that is the bandwidth of the inner loop is increased, the system becomes critical stable and then stable as shown in Fig.9 (a). However, the **C2** method can only obtain the conclusion of stability but cannot obtain the conclusion of critical stability according to $G_2(s)$ and $G_3(s)$ in (19).

With the increase of ε that is the bandwidth of the outer loop is increased, the oscillation amplitude becomes larger correspondingly as Fig.9 (b) shows. The oscillation amplitude with $\varepsilon = 0.1$ is very small and can be neglected, but the oscillation amplitude with $\varepsilon = 1$ is relatively large, which is

$$A_3 = 64 \text{ kW}, w_3 = 221 \text{ rad/s}. \quad (20)$$

Compared to the oscillation amplitude A_1 and frequency w_1 with $\varepsilon = 0.5$ shown in (18), the oscillation amplitude increases two times but the frequency keeps unchanged. Obviously, the **C2** method ignores the influence of P&O based power control and thus cannot analyze the influence of ε.

In conclusion, when the bandwidth of the outer loop is bigger and the bandwidth of the inner loop is smaller, the system is easier to be unstable.

C. Filters

This part mainly studies the influence of the filters. First, the influence of the capacitance across the PV terminal C_{pv} is studied. When $C_{pv} = 1$ mF, 1.5 mF, 1.9 mF in sequence, the corresponding Nyquist diagrams are depicted in Fig.10 (a). Through the figure, it can be seen that C_{pv} can greatly influence the dynamics of the system. When $C_{pv} = 1$ mF, the oscillation can be neglected. But when $C_{pv} = 1.9$ mF, the oscillation becomes very large, whose amplitude and frequency are

$$A_3 = 207 \text{ kW}, w_3 = 193 \text{ rad/s}. \quad (21)$$

Comparing A_1, w_1 in (18) and A_3, w_3 in (21), it can be concluded that the oscillation amplitude changes greatly, but oscillation frequency changes a little.

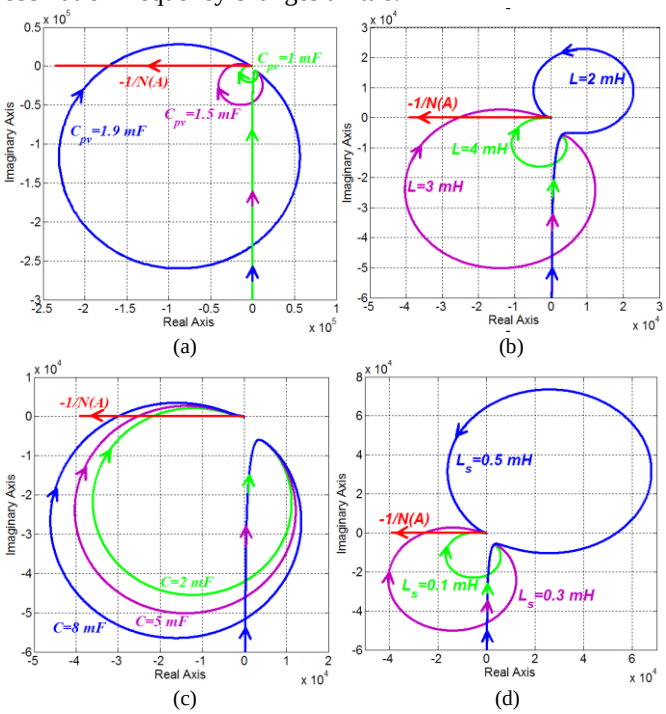

(a) (b) (c) (d)

Fig.10. Nyquist diagram of the system with changes of filters. (a) C_{pvP}=1, 1.5, 1.9 mF. (b) L=4, 3, 2 mH. (c) C=2, 5, 8 mF. (d) L_s=0.1, 0.3, 0.5 mH.

When the inductance of the LC filter $L = 4, 3, 2$ mH in sequence, the corresponding Nyquist diagrams are depicted in Fig.10 (b). It can be seen that if L increases, the system stability can be enhanced. But if L decreases, the oscillation becomes more obvious and even unstable like $L = 2$ mH. When $L = 2$ mH, the corresponding transfer functions $G(s)$of the linear part is

$$G_3 = \frac{8.1*10^8(s+420.8)(s+266.7)(s+66.67)(s^2+110.1s+7.51*10^5)}{s(s+4406)(s+48.98)(s^2-24.79s+4.7*10^4)(s^2+622.7s+7.26*10^5)}. \quad (22)$$

That is, $G_3(s)$ have unstable poles, hence, the system is unstable when $L = 2$ mH. Based on (16) and (22), the instability conclusion can be also obtained through **C2** method.

When the capacitance of the LC filter $C = 2, 5, 8$ mF in sequence, the corresponding Nyquist diagrams are depicted in Fig.10 (c). Through the figure, it can be found that C has small influence on the dynamics of the system.

When the impedance of the grid side $L_s = 0.1, 0.3, 0.5$ mH in sequence, the corresponding Nyquist diagrams are depicted in Fig.10 (d). From the results, it can be found that with the increase of L_s, the system stability degrades. When $L_s = 0.5$ mH, the system is unstable. At the moment, the transfer functions $G(s)$of the linear part is

$$G_3 = \frac{8.1*10^8(s+275.7)(s+266.7)(s+66.67)(s^2+73.79s+4.59*10^5)}{s(s+3187)(s+48.22)(s^2-8.54s+4.6*10^4)(s^2+577.9s+4.2*10^5)}. \quad (23)$$

This article has been accepted for publication in a future issue of this journal, but has not been fully edited. Content may change prior to final publication. Citation information: DOI 10.1109/TIE.2018.2864695, IEEE Transactions on Industrial Electronics

Therefore, through **C2** method, the same conclusion can be obtained.

In conclusion, the filters can influence the dynamics of the PV generator with different sensitivities. Furthermore, improper filters will cause the instability of the system.

V. HARDWARE-IN-LOOP TESTS

To verify the effectiveness of the theoretical analyses, the corresponding hardware-in-loop (HIL) tests are conducted using the RTLAB and TMS320F28335 DSP. The equipment of the HIL tests is shown in Fig.11, where the main loop shown in Fig.4 is simulated in RTLAB and control algorithm is realized through the 28335 DSP. The rated electrical and control parameters are the same as Table Ⅰ.

Fig.11. HIL tests setup.

Fig.12 shows the output power and PV voltage of the PV generator with changes of operation points and control parameters. Fig. 12 (a) shows the dynamics of the system with changes of perturbation size ε when operation points are (180 kW, 731 V) and (160 kW, 650 V). It can be seen that with the increase of ε which means the equivalent bandwidth of the outer loop is increasing, both the output power and PV voltage oscillate more obviously. Through the enlarged version in Fig.12 (b), the oscillation amplitude and frequency can be obtained. When $\varepsilon = 1, 0.5$ V in sequence, the oscillation amplitudes are about 55 kW and 31 kW respectively, while frequency is about 225 rad/s and almost kept unchanged. These results can meet the theoretical calculation in (18) and (20). Relatively speaking, $\varepsilon = 0.5$ V is more consistent with the theoretical calculation, because oscillation is relatively smaller than that of $\varepsilon = 1$ V, which more meets the assumption of the small-signal model. Furthermore, when the operation point moves left from (180 kW, 731 V) to (160 kW, 650 V), the stability degrades and the oscillation is more obvious. It should be noted that these changes are caused by the system stability but not coefficient k ($\Delta P_{pv} = k\Delta v_{pv}$), actually, k at these two operation points is almost the same. Based on the conventional **C2** method, the critical stable situations cannot be analyzed and corresponding oscillation information cannot be obtained.

Fig.12 (c) shows the dynamics of the system with changes of ε when operation points are (180 kW, 1253 V) and (160 kW, 1264 V). It can be seen that there is no obvious oscillation and changes of ε almost have no influence on the stability of the system. That is, the system stability can be improved a lot when the operation points are located on the right side.

Fig.12 (d) shows the dynamics of the system with changes of k_{pvP} at the rated operation point. From the results, it can be found that with the decreases of k_{pvP} that is the equivalent bandwidth of the inner loop is decreasing, the system is more and more unstable. There is no obvious oscillation when $k_{pvP} = 0.3$ but the system is unstable when $k_{pvP} = 0.1$, which meets the theoretical analysis well. The unstable situation can be obtained by the **C2** method too.

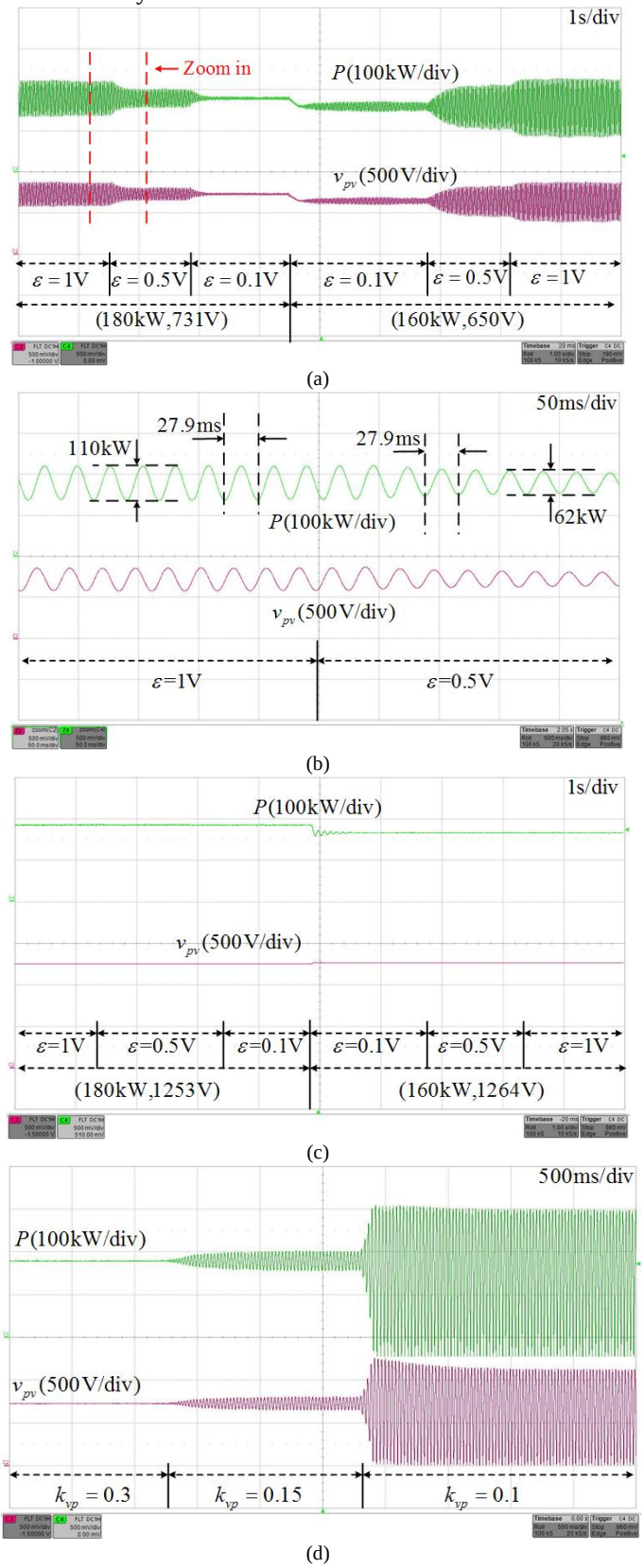

Fig.12. Dynamics of the system with changes of operation points and control parameters. (a) ε changes with operation points on the left side . (b) Enlarged version of (a). (c) ε changes with operation points on the right side. (d) k_{pvP} changes.

This article has been accepted for publication in a future issue of this journal, but has not been fully edited. Content may change prior to final publication. Citation information: DOI 10.1109/TIE.2018.2864695, IEEE Transactions on Industrial Electronics

In conclusion, the system stability can be enhanced if operation points are located on the right side and the bandwidth of the outer loop is much smaller than that of the inner loop.

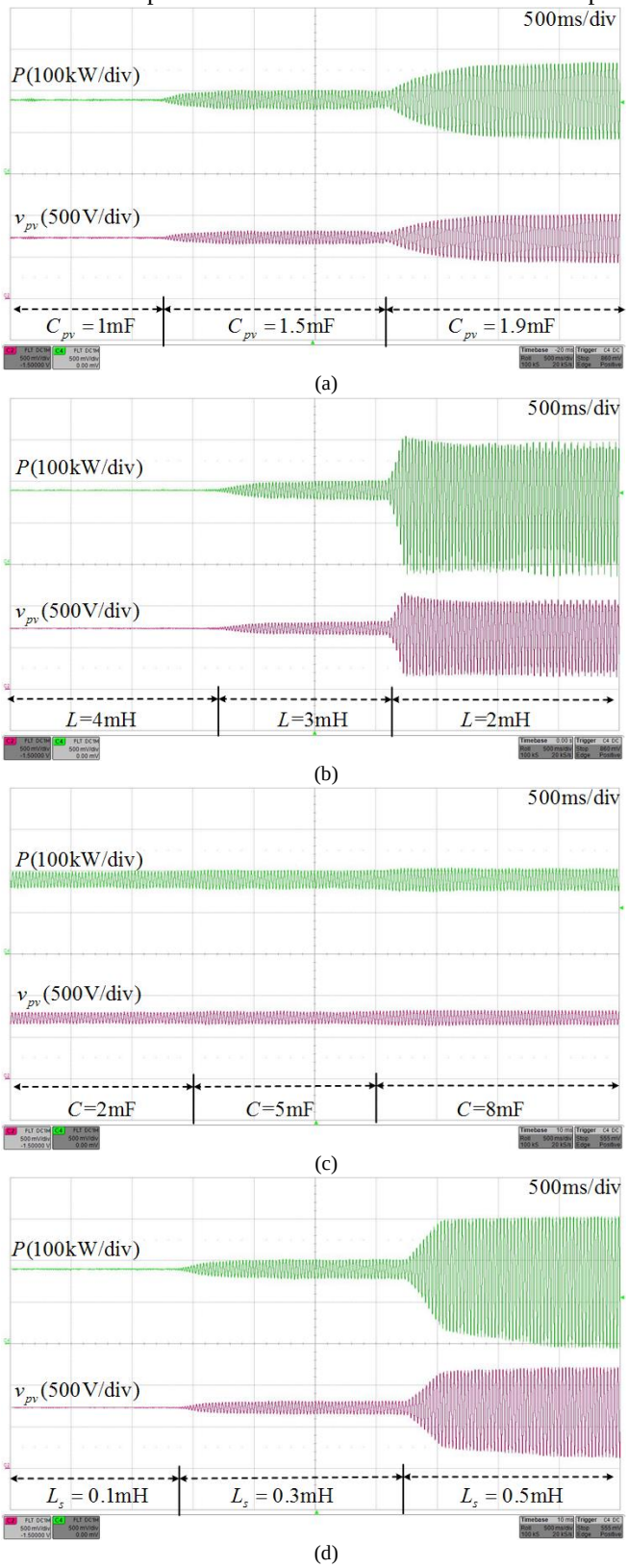

Fig.13. Dynamics of the system with changes of filters. (a) C_{pv} changes. (b) L changes. (c) C changes. (d) L_s changes.

Fig.13 shows the output power and PV voltage of the PV generator with changes of filters. Fig.13 (a) shows the influence of the capacitance across the PV terminal C_{pv}. When C_{pv} = 1mF, there is no obvious oscillation. But with the increase of C_{pv}, the oscillation becomes stronger and stronger. Especially when C_{pv} = 1.9 mF , although the system is not collapsed, the oscillation amplitude is very big, which greatly influences the safety of the system. Similarly, the **C2** method cannot effectively analyze the corresponding critical stable situations.

Fig.13 (b) and (c) show the influence of the LC filter. It can be seen that the influence of inductance L is greater than the capacitance C. With the decrease of L, the system will be critical stable and then unstable. But with the increase of C, the oscillation amplitude increases slightly. This can be effectively explained by the corresponding theoretical analysis.

Fig.13 (d) shows the influence of the impedance of the grid side L_s. Through the figure, it can be seen that with the increase of L_s, the system will be gradually critical stable (0.3 mH)and then unstable (0.5 mH). Therefore, it can be concluded that the system is more stable with smaller L_s.

VI. Conclusion

In this paper, the DF method is applied to analyze the stability of PV generators with consideration of nonlinear discontinuous P&O based power control, which makes the conventional small-signal analysis not suitable anymore. Through modeling in the frequency domain, the discontinuity of the P&O based power control is overcome. Then, based on the modified Nyquist criterion, the stability of the PV generator is carefully studied considering many different influence factors including operation points, control parameters and filters. It is concluded that stability can be enhanced through:

1) Operation points should be located on the right side.

2) The bandwidth of the outer loop should be much smaller than that of the inner loop.

3) Proper filters should be designed with tradeoff between performance and stability (smaller C_{pv}, larger L and smaller L_s).

Furthermore, by the contrastive analysis, it is found that the results will be not accurate if the influence of P&O based power control is not considered especially for the critical stable situation. On the other hand, through the constructed analysis method, more accurate guidance for the parameter design can be provided. At last, the results of HIL tests can effectively verify all the theoretical analyses.

References

[1] H. Xin, Z. Qu, J. Seuss and A. Maknouninejad, "A Self-Organizing Strategy for Power Flow Control of Photovoltaic Generators in a Distribution Network," *IEEE Trans. Power Syst.*, vol. 26, no. 3, pp.1462-1473, Aug. 2011.

[2] K. Kawabe and K. Tanaka, "Impact of Dynamic Behavior of Photovoltaic Power Generation Systems on Short-Term Voltage Stability," *IEEE Trans. Power Syst.*, vol. 30, no. 6, pp. 3416-3424, Nov. 2015.

[3] C. Zhang, S. Du and Q. Chen, "A Novel Scheme Suitable for High-Voltage and Large-Capacity Photovoltaic Power Stations," *IEEE Trans. Ind. Electron.*, vol. 60, no. 9, pp. 3775-3783, Sept. 2013.

[4] Y. Xia, W. Wei, Y. Peng, P. Yang and M. Yu, "Decentralized Coordination Control for Parallel Bidirectional Power Converters in a Grid-Connected DC Microgrid," *IEEE Trans. Smart Grid*, vol. PP, no. 99, pp. 1-1.

[5] C. Rodriguez and J. D. K. Bishop, "Organic Architecture for Small- to Large-Scale Photovoltaic Power Stations," *IEEE Trans. Ind. Electron.*, vol. 56, no. 11, pp. 4332-4343, Nov. 2009.

[6] Yun Tiam Tan, D. S. Kirschen and N. Jenkins, "A model of PV generation suitable for stability analysis," *IEEE Trans. Energy Convers.*, vol. 19, no. 4, pp. 748-755, Dec. 2004.

[7] B. Wen, D. Boroyevich, R. Burgos, P. Mattavelli and Z. Shen, "Analysis of D-Q Small-Signal Impedance of Grid-Tied Inverters," *IEEE Trans. Power Electron.*, vol. 31, no. 1, pp. 675-687, Jan. 2016.

[8] J. Fang, X. Li, H. Li and Y. Tang, "Stability Improvement for Three-Phase Grid-Connected Converters through Impedance Reshaping in Quadrature-Axis," *IEEE Trans. Power Electron.*, vol. PP, no. 99, pp. 1-1.

[9] Y. Xia, Y. Peng and W. Wei, "Triple droop control method for ac microgrids," *IET Power Electron.*, vol. 10, no. 13, pp. 1705-1713, Oct. 2017.

[10] L. Guo, S. Zhang, X. Li, Y. W. Li, C. Wang and Y. Feng, "Stability Analysis and Damping Enhancement Based on Frequency-Dependent Virtual Impedance for DC Microgrids," *IEEE J. Emerg. Sel. Topics Power Electron.*, vol. 5, no. 1, pp. 338-350, Mar. 2017.

[11] A. Kwasinski and C. N. Onwuchekwa, "Dynamic Behavior and Stabilization of DC Microgrids With Instantaneous Constant-Power Loads," *IEEE Trans. Power Electron.*, vol. 26, no. 3, pp. 822-834, March 2011.

[12] M. Su, Z. Liu, Y. Sun, H. Han and X. Hou, "Stability Analysis and Stabilization Methods of DC Microgrid With Multiple Parallel-Connected DC－DC Converters Loaded by CPLs," *IEEE Trans. Smart Grid*, vol. 9, no. 1, pp. 132-142, Jan. 2018.

[13] A. P. N. Tahim, D. J. Pagano, E. Lenz and V. Stramosk, "Modeling and Stability Analysis of Islanded DC Microgrids Under Droop Control," *IEEE Trans. Power Electron.*, vol. 30, no. 8, pp. 4597-4607, Aug. 2015.

[14] Z. Moradi-Shahrbabak and A. Tabesh, "Effects of Front-End Converter and DC-Link of a Utility-Scale PV Energy System on Dynamic Stability of a Power System," *IEEE Trans. Ind. Electron.*, vol. 65, no. 1, pp. 403-411, Jan. 2018.

[15] A. A. A. Radwan and Y. A. R. I. Mohamed, "Power Synchronization Control for Grid-Connected Current-Source Inverter-Based Photovoltaic Systems," *IEEE Trans. Energy Convers.*, vol. 31, no. 3, pp. 1023-1036, Sept. 2016.

[16] L. Wang, Q. S. Vo and A. V. Prokhorov, "Stability Improvement of a Multimachine Power System Connected With a Large-Scale Hybrid Wind-Photovoltaic Farm Using a Supercapacitor," *IEEE Trans. Ind. Appl.*, vol. 54, no. 1, pp. 50-60, Jan. 2018.

[17] L. Wang, Q. S. Vo and A. V. Prokhorov, "Dynamic Stability Analysis of a Hybrid Wave and Photovoltaic Power Generation System Integrated Into a Distribution Power Grid," *IEEE Trans. Sustain. Energy*, vol. 8, no. 1, pp. 404-413, Jan. 2017.

[18] S. Liu, P. X. Liu and X. Wang, "Stochastic Small-Signal Stability Analysis of Grid-Connected Photovoltaic Systems," *IEEE Trans. Ind. Electron.*, vol. 63, no. 2, pp. 1027-1038, Feb. 2016.

[19] S. Liu, P. X. Liu and X. Wang, "Stability Analysis of Grid-Interfacing Inverter Control in Distribution Systems With Multiple Photovoltaic-Based Distributed Generators," *IEEE Trans. Ind. Electron.*, vol. 63, no. 12, pp. 7339-7348, Dec. 2016.

[20] R. Haroun, A. E. Aroudi, A. Cid-Pastor, G. Garcia, C. Olalla and L. Martínez-Salamero, "Impedance Matching in Photovoltaic Systems Using Cascaded Boost Converters and Sliding-Mode Control," *IEEE Trans. Power Electron.*, vol. 30, no. 6, pp. 3185-3199, Jun. 2015.

[21] D. Engels, "The describing functions for a constrained-range integration process with bang-bang input and dead zone," *IEEE Trans. Autom. Control*, *vol.* 12, no. 5, pp. 582–585, Oct. 1967.

[22] H. Li, S. Wang, J. Lü, X. You and X. Yu, "Stability Analysis of the Shunt Regulator With Nonlinear Controller in PCU Based on Describing Function Method," *IEEE Trans. Ind. Electron.*, vol. 64, no. 3, pp. 2044-2053, Mar. 2017.

[23] A. Sangwongwanich, Y. Yang and F. Blaabjerg, "High-Performance Constant Power Generation in Grid-Connected PV Systems," *IEEE Trans. Power Electron.*, vol. 31, no. 3, pp. 1822-1825, March 2016.

[24] H. D. Tafti, A. I. Maswood, G. Konstantinou, J. Pou and F. Blaabjerg, "A General Constant Power Generation Algorithm for Photovoltaic Systems," *IEEE Trans. Power Electron.*, vol. 33, no. 5, pp. 4088-4101, May 2018.

[25] M. G. Villalva, J. R. Gazoli and E. R. Filho, "Comprehensive Approach to Modeling and Simulation of Photovoltaic Arrays," *IEEE Trans. Power Electron.*, vol. 24, no. 5, pp. 1198-1208, May 2009.

[26] H. Cai, J. Xiang and W. Wei, "Decentralized Coordination Control of Multiple Photovoltaic Sources for DC-bus Voltage Regulating and Power Sharing," *IEEE Trans. Ind. Electron.*, vol. PP, no. 99, pp. 1-1.

Yanghong Xia (S'16) received the B.S. degree in automation from the College of Automation, Huazhong University of Science and Technology, Wuhan, China, in 2014. Now he is working toward the Ph.D. degree in the College of Electrical Engineering, Zhejiang University, Hangzhou, China.

His current research interests include advanced control methods, stability analysis of power system, hybrid ac/dc microgrids.

Wei Wei received the B.Eng. degree in automation, M.Eng. degree in control theory and control engineering, and D.Eng. degree in power electronics and electronic drives all from the College of Electrical Engineering, Zhejiang University, China, in 1983, 1986 and 1994, respectively. Now he is a professor in the College of Electrical Engineering, Zhejiang University.

His currently research interests includes intelligent control, the development of novel technology of renewable energy and smart grid.

Miao Yu (M'16) received the B.S. degree in Automation from College of Electrical Engineering, Zhejiang University, China in 2007. Then he received Ph.D. degree in Control Science and Engineering from the same university in 2012. From 2013 to 2015, he was working in Aalto University, Finland as a postdoctoral researcher.

Since 2016, he has been working in College of Electrical Engineering, Zhejiang University, China as an associate professor. He has authored or coauthored more than 20 technical papers in journal and conferences. His current research interests include control strategies in microgrid and renewable power generation.

Peng Wang (M'00-SM'11-F'18) received his B.Sc. degree from Xian Jiaotong University, China, in 1978, the M. Sc. degree from Taiyuan University of Technology, China, in 1987, and the M. Sc. and Ph.D. degrees from the University of Saskatchewan, Canada, in 1995 and 1998 respectively. Currently, he is a professor of Nanyang Technological University, Singapore.